



**HAL**  
open science

## Voltammetric and microscopic characteristics of MnO<sub>2</sub> and silica-MnO<sub>2</sub> hybrid films electrodeposited on the surface of planar electrodes

Anastasiia Kovalyk, Oksana Tananaiko, Anna Borets, Mathieu Etienne, Alain Walcarius

► **To cite this version:**

Anastasiia Kovalyk, Oksana Tananaiko, Anna Borets, Mathieu Etienne, Alain Walcarius. Voltammetric and microscopic characteristics of MnO<sub>2</sub> and silica-MnO<sub>2</sub> hybrid films electrodeposited on the surface of planar electrodes. *Electrochimica Acta*, 2019, 306, pp.680-687. 10.1016/j.electacta.2019.03.156 . hal-02089714

**HAL Id: hal-02089714**

**<https://hal.univ-lorraine.fr/hal-02089714v1>**

Submitted on 26 Nov 2020

**HAL** is a multi-disciplinary open access archive for the deposit and dissemination of scientific research documents, whether they are published or not. The documents may come from teaching and research institutions in France or abroad, or from public or private research centers.

L'archive ouverte pluridisciplinaire **HAL**, est destinée au dépôt et à la diffusion de documents scientifiques de niveau recherche, publiés ou non, émanant des établissements d'enseignement et de recherche français ou étrangers, des laboratoires publics ou privés.

# **Voltammetric and microscopic characteristics of MnO<sub>2</sub> and silica-MnO<sub>2</sub> hybrid films electrodeposited on the surface of planar electrodes**

Anastasiia Kovalyk<sup>a</sup>, Oksana Tananaiko<sup>a</sup>, Anna Borets<sup>a</sup>, Mathieu Etienne<sup>b</sup>, Alain Walcarius<sup>b</sup>

<sup>a</sup> *Kyiv National Taras Shevchenko University, Volodymirska street 64, Kyiv 01601, Ukraine*

<sup>b</sup> *Université de Lorraine and CNRS, Laboratoire de Chimie Physique et Microbiologie pour les Matériaux et l'Environnement, UMR7564, 405 rue de Vandœuvre, 54600 Villers-lès-Nancy, France*

**Abstract:** The morphological and electrocatalytic properties of ITO and nanostructured carbon screen printed electrodes (nanoSPCE) modified with thin films of MnO<sub>2</sub> particles, alone or as hybrid with SiO<sub>2</sub>, as obtained using electrodeposition techniques, were studied. The time and potential of MnO<sub>2</sub> electrodeposition influenced the electrocatalytic properties of the modified electrodes towards H<sub>2</sub>O<sub>2</sub>. The highest electrocatalytic current was observed at deposition potential E = -0.8 V and deposition time of 10 s. MnO<sub>2</sub> particles with uniform distribution were obtained onto the electrode surface when prepared under optimal conditions. The nanoSPCE-MnO<sub>2</sub> has demonstrated larger effective surface area and faster charge transfer rates compared to ITO-MnO<sub>2</sub>. The electrodeposited silica, in addition to MnO<sub>2</sub>, improved the operational stability of the electrodes without noticeable decreasing of their performance. Modified electrodes were used for hydrogen peroxide determination.

**Keywords:** ITO electrodes, carbon nanostructured screen printed electrodes, MnO<sub>2</sub> particles, silica films, electrochemical deposition, voltammetry, hydrogen peroxide.

## 1. Introduction

The development of sensitive elements of disposable amperometric sensors for medical diagnostics or on-site analyses is an important task of the modern analytical chemistry [1,2]. The planar printed electrodes are perspective for this purpose. Many commercial biosensors are based on electron mediator transport [3,4]. Metal and metal oxide nanoparticles immobilized on electrode surfaces can act as electro mediators in amperometric enzymatic sensors [2,5], and they can be even used for the development of enzymatic free sensors [6-10].

Because hydrogen peroxide is a common product of many enzymatic transformations, the development of the sensitive elements of amperometric sensors for  $H_2O_2$  is a challenge for the construction of several enzymatic biosensors. The nanoparticles of noble metals (Au, Pt) are commonly used catalysts in amperometric sensors for hydrogen peroxide, thanks to their high activity and stability [1]. However, there are other more available and low cost mediators, such as transition metal oxide particles, i.e.  $MnO_2$ .

$MnO_2$  is known as mediator for hydrogen peroxide amperometric detection [7-11]. In particular,  $MnO_2$  nanoparticles can be reduced by  $H_2O_2$  on carbon, gold or ITO electrodes to Mn(II) or Mn(III) species and then re-oxidized to  $MnO_2$  electrochemically [10-12]. The resulting anodic currents sampled at the electrode increased proportionally to  $H_2O_2$  content in solution. The selectivity and sensitivity of  $H_2O_2$  detection using an electrode modified with  $MnO_2$  catalyst were improved compared to the bare one [8,10]. The use of  $MnO_2$  as electron mediator is a good alternative to gold or platinum nanoparticles.

The presence of reducing agents such as ascorbic acid or urea can influence the results of hydrogen peroxide determination, which is a problem for amperometric enzymatic sensors. The oxidation currents of the mentioned compounds appear indeed at potential values overlapping with  $H_2O_2$  signals, which caused an error in the results of determination of  $H_2O_2$ . In the goal to circumvent this limitation,  $MnO_2$  powder was used to reduce the influence of ascorbic acid on the results of choline amperometric determination with a help of the electrode modified with choline

oxidase [13-15]. Ascorbic acid was oxidized during the pretreatment of the solution with  $\text{MnO}_2$  particles. To avoid such pretreatment with addition of  $\text{MnO}_2$  particles into the solution, it would be interesting to use an electrode modified with  $\text{MnO}_2$  particles immobilized onto its surface for the development of the sensor element for amperometric determination of  $\text{H}_2\text{O}_2$  in the presence of reducing agents such as ascorbic acid. The rate of ascorbic acid oxidation onto  $\text{MnO}_2$  should be lower than the catalytic oxidation of  $\text{H}_2\text{O}_2$ . Indium tin oxide (ITO) based electrodes can possess good affinity to  $\text{MnO}_2$  particles and thus ensure better holding of the particles on its surface, owing to favorable interactions between ITO and metal oxide particles [16-20]. Carbon electrodes might be also of interest because they offer relatively easy surface modification platforms for mediators [21].

The use of screen printed electrodes is important for the development of portable disposable sensors. It was demonstrated earlier that carbon screen printed electrodes modified with enzymes were successfully applied for the construction of amperometric biosensors for determination of choline [15, 22],  $\text{H}_2\text{O}_2$  and phenols [19, 21], L-ascorbic acid [23], glutamate [24], biogenic amines [25] and glucose [26]. The immobilization of nanostructured materials together with enzymes onto the surface of the screen printed electrodes is also a perspective for the development of third generation biosensors [18-20].

In the present work we studied nanostructured screen printed carbon electrodes (nanoSPCE), which possess higher surface area compared to carbon screen printed electrodes described earlier. Such electrodes can be perspective sensitive elements of amperometric sensors. The modification of nanoSPCE with  $\text{MnO}_2$  particles and their application for  $\text{H}_2\text{O}_2$  determination was not yet investigated to our knowledge.

$\text{MnO}_2$  particles can be synthesized in solution and then immobilized onto an electrode surface in the form of thin films using organic or inorganic binders [10,12,16]. Beside this,  $\text{MnO}_2$  films can be directly electrodeposited onto the surface of the electrode from a solution containing  $\text{Mn(II)}$  species by applying a positive potential to the working electrode [27-29]. Good control of

the amount and size of the metal oxide particles on the electrode surface can be achieved by controlling the electrodeposition parameters (applied potential and deposition time).

On the other hand, sol-gel-derived silica films can be generated on solid electrodes by the electrochemically-assisted deposition (EAD) method, which is also a convenient procedure for the immobilization and holding of nanoparticles and enzymes onto electrode surfaces [30-37]. The method is easy to use, it is quick and it allows to control the thickness and surface characteristics of SiO<sub>2</sub> on the electrode by adjusting the time and value of applied potential [37-40]. The EAD method allows precise modification of the target electrode because the catalyst is being generated only in close vicinity of negatively-polarized (working) electrode. Recently this procedure was successfully applied for the modification of screen printed planar electrode with biocomposite film silica-choline oxidase [22]. It was also used to generate extremely porous coatings by adding surfactants in the synthesis medium [31,38,41-43], which can be otherwise applied as a useful matrix to encapsulate functional microparticles in a durable way (e.g., clays [44]).

The objective of the work is modification of the nanoSPCE and ITO electrodes with MnO<sub>2</sub> particles using direct electrodeposition technique followed by their coating/embedding with a silica film generated by EAD method. The comparison of the electrocatalytic characteristics of obtained modified electrodes using H<sub>2</sub>O<sub>2</sub> as a model substrate is then made in respect to their further application as sensitive elements of amperometric sensors.

## **2. Experimental section**

### *2.1. Materials, Reagents and Apparatus*

Tetraethoxysilane (TEOS, 98%) was purchased from Fluka (Switzerland). Cetyltrimethylammonium bromide (CTAB) was provided by Sigma (USA). Phosphate buffer solutions (PBS) were prepared from Na<sub>2</sub>HPO<sub>4</sub>·2H<sub>2</sub>O and KH<sub>2</sub>PO<sub>4</sub> (99.5%, Merck, Germany). All the other reagents were of analytical grade. All solutions were prepared using doubly distilled water. The nanoSPCE ensembles were made of a nanostructured carbon screen-printed working

electrode, a carbon counter-electrode and an AgCl reference electrode, which were purchased from Orion Technology (OHT-000). The working electrode (WE) was obtained using carbon nanoparticles-based inks. The size of carbon nanoparticles constituting the electrode was in the 20-60 nm range according to the manufacturer. The diameter of the WE was 4 mm. For comparison purposes, a classical carbon screen printed electrode (SPCE, purchased from Ital Sens) was tested. In this case, the WE (3 mm in diameter) was obtained from carbon inks without particles size control.

Glass slides covered with an ITO film (1.1 mm thickness) were used as ITO electrodes (Sigma-Aldrich); a Pt wire and Ag/AgCl were used as counter and reference electrodes, respectively. All electrochemical experiments were conducted using either a model  $\mu$ Stat400 bipotentiostat/galvanostat (DropSens, Spain) or a EmStat2 potentiostat (Palm-Sens, Netherlands). SEM measurements of MnO<sub>2</sub> and ITO modified with MnO<sub>2</sub> were carried out using the model JCM-6000 scanning electron microscope (JEOL).

### *2.2. Electrochemical deposition of MnO<sub>2</sub> onto electrode surfaces*

Synthesis of manganese dioxide particles was carried out by electrochemical deposition in accordance with the method described in [16]. For this purpose, ITO and nanoSPCE electrodes were immersed in a solution of 0.05M MnSO<sub>4</sub> and 0.1M CH<sub>3</sub>COOK and a constant potential (typically between +0.6 and +1.0 V) was applied to the working electrode: the time of such potentiostatic electrodeposition was varied in the range of 10-240 s (see optimization detail at section 3.2). Obtained modified electrodes, respectively ITO-MnO<sub>2</sub> and nanoSPCE-MnO<sub>2</sub>, were dried in an oven at 100<sup>0</sup>C for 5 hours and then kept at room temperature for 12 hours prior to use.

### *2.3. Modification of the electrodes with SiO<sub>2</sub> film*

The ITO-MnO<sub>2</sub> and nanoSPCE-MnO<sub>2</sub> electrodes were then modified with silica film using EAD method [37,44]. The composition of the sol for deposition was adapted from the literature [22,37]: the acidic hydrolysis of tetraethoxysilane was performed by mixing TEOS, H<sub>2</sub>O and 0.01M HCl with the volume ratio 1.4 : 1:1.73 for 8 hours. Then a calculated amount of CTAB was

added to obtain 1mM solution of surfactant in the final sol, 0.3 mL of 67 mM PBS (pH 7.0). The mixture was carefully mixed and 50  $\mu$ L were dropped on the sensitive part of screen printed chip covering all three electrodes. The negative potential ( $E = -1.1$  V) was applied to the working electrode for 15 s. In the case of modification of ITO electrodes they were dipped into the mixture of silica sol then the same potential of -1.1 V was applied for 15 s. After film formation, the electrodes were left for 1 min covered with sol, then carefully washed with water and dried at room temperature for 30 min. The obtained modified electrodes (ITO-MnO<sub>2</sub>-SiO<sub>2</sub> and nanoSPCE-MnO<sub>2</sub>-SiO<sub>2</sub>) were kept at room temperature for 8 hours and washed with phosphate buffer pH-8.0 for 30 min prior to use. They were stored in desiccator if not in use.

### 3. Results and discussion

#### *3.1. Electrochemical response of MnO<sub>2</sub> modified electrodes toward H<sub>2</sub>O<sub>2</sub>.*

Before investigating the effect of MnO<sub>2</sub> on the cyclic voltammetric (CV) response of H<sub>2</sub>O<sub>2</sub> (i.e., using nanoSPCE and ITO electrodes modified with MnO<sub>2</sub> particles), some preliminary experiments were performed on bare screen-printed carbon electrodes (i.e., inks containing carbon nanoparticles or not) in order to select the most promising one for further experiments. The CV curves recorded in the absence and presence of hydrogen peroxide at the bare carbon screen printed electrode (CSPE) and at the nanostructured carbon screen printed electrode (nanoSPCE) were compared (Fig. 1a). Both background and oxidation currents of H<sub>2</sub>O<sub>2</sub> are much higher at the nanostructured carbon electrode (curves 3&4), and the presence of H<sub>2</sub>O<sub>2</sub> was even not noticeable on classical (i.e., not nanostructured) screen-printed electrode (curves 1&2 superimposed). The overpotential for H<sub>2</sub>O<sub>2</sub> oxidation was much less at the nanoSPCE, indicating its interest for further modification with MnO<sub>2</sub>.

The typical CV response of the nanoSPCE after electrodeposition of MnO<sub>2</sub> (nanoSPCE-MnO<sub>2</sub>) is presented in Fig. 1b, curve 1. The small signals observed in the buffer solution can be attributed to the Mn(IV) / Mn(III), Mn(II) redox systems in their oxide states, as described previously [10,

46]. As no peak current was observed at unmodified nanoSPCE, these results confirm the presence of Manganese species on the surface of the nanoSPCE. Anodic current of nanoSPCE-MnO<sub>2</sub> at E = 0.6 V noticeably increases in the presence of 1·10<sup>-3</sup> M H<sub>2</sub>O<sub>2</sub> (Fig 1b, curve 2). This is due to the electrocatalytic oxidation of H<sub>2</sub>O<sub>2</sub> at nanoSPCE-MnO<sub>2</sub> which was described earlier for the other types of the electrodes modified with MnO<sub>2</sub> [10,11].

Please insert here Figs. 1a, 1b & 2a, 2b

A similar set of CV experiments has been performed with ITO electrodes, respectively before and after electrodeposition of MnO<sub>2</sub>, in the absence and presence of H<sub>2</sub>O<sub>2</sub>, as presented in Fig. 2. Two slightly visible oxidation- reduction peaks at E 0.4 and 0.3 V can be noticed in CV recorded in the background electrolyte at bare ITO (Fig 2a, curve 1), possibly due to some impurities in solution. A well-defined oxidation peak at E = 0.7 V appeared in the presence of H<sub>2</sub>O<sub>2</sub> in solution (Fig. 2a, curve 2). Much larger peak currents were observed when using the MnO<sub>2</sub>-modified ITO electrode either with or without H<sub>2</sub>O<sub>2</sub> (Fig. 2b). The two well defined oxidation-reduction peaks observed at ITO-MnO<sub>2</sub> (at +0.65 and +0.4 V, respectively) in phosphate buffer at pH 8.0 (Fig. 2b, curve 2) confirm the presence of MnO<sub>2</sub> on the ITO surface and testify that MnO<sub>2</sub> is electrochemically active. The oxidation current of ITO-MnO<sub>2</sub> at E = 0.65 V noticeably increased in the presence of hydrogen peroxide while the reduction current was not changed (Fig. 2b, curve 2). As for nanoSPCE-MnO<sub>2</sub>, this is the result of the catalytic oxidation of H<sub>2</sub>O<sub>2</sub> at ITO-MnO<sub>2</sub>, but the difference between the CV curves (peak current ratio) recorded in the background electrolyte and in the presence of 1·10<sup>-3</sup> M H<sub>2</sub>O<sub>2</sub> is more clear at nanoSPCE-MnO<sub>2</sub>.

### *3.2. Optimization studies of MnO<sub>2</sub> electrodeposition.*

It was investigated the influence of the deposition potential, time and concentration of Mn(II) solution on the electrocatalytic properties of the studied electrodes. The oxidation current of H<sub>2</sub>O<sub>2</sub> at nanoSPCE-MnO<sub>2</sub> and ITO-MnO<sub>2</sub> was used as analytical signal.

*Effect of electrodeposition potential.* The deposition potential of MnO<sub>2</sub> at nanoSPCE and ITO electrodes was varied in the range of +0.6 to +1.0 V. The range of potentials is limited by the



value of the formal redox potential of the (Mn (IV) / Mn (II) system ( $E = 0.72$  V at pH 8.0) and the beginning of water decomposition at  $E = 1.0$  V. The optimal electrodeposition potential of  $\text{MnO}_2$  on the both nanoSPCE and ITO electrodes was  $+0.8$  V, leading to the highest analytical signal observed for  $\text{H}_2\text{O}_2$  detection (please see supplementary material, Fig. 1S).

*Effect of the modifier precursor concentration.* The concentration of the  $\text{MnSO}_4$  solution used for electrodeposition process was varied in the range of 0.05 - 0.5 M. The oxidation potential of  $\text{H}_2\text{O}_2$  depended of the concentration of  $\text{MnSO}_4$ , and increased from 0.65 to 0.8 V when passing from more diluted to more concentrated solutions. 0.05 M solution of  $\text{MnSO}_4$  was thus used further for electrode modification as it gave rise to the best electrocatalytic behavior (the oxidation potential of  $\text{H}_2\text{O}_2$  was the lowest in this case, please see supplementary material, Fig. 2S).

*Effect of electrodeposition time.* The time of electrodeposition of  $\text{MnO}_2$  onto ITO electrodes was checked in the range of 10 - 240 s. In agreement with previous observations [10], varying the the deposition time causes the formation of either  $\text{MnO}_2$  particles or films on the surface of the electrodes. Increasing the deposition time from 10 to 240 s resulted in an anodic shift in the oxidation potential of hydrogen peroxide, from 0.65 to 0.85 V (please see supplementary material, Fig. 3S).

In conclusion, the highest electrocatalytic current for  $\text{H}_2\text{O}_2$  oxidation and the lowest potential values was observed for the electrodes modified with  $\text{MnO}_2$  particles generated from 0.05 M solution of  $\text{MnSO}_4$  (in 0.1M  $\text{CH}_3\text{COOK}$ ) at a deposition potential of  $E = +0.8$  V and deposition times of 10 – 60 s.

The SEM micrographs of ITO electrode modified with  $\text{MnO}_2$  from 0.05 M  $\text{MnSO}_4$  at potential  $E = +0.8$  V for various deposition times are presented in Fig. 3. Uniformly distributed disaggregated particles are observed on the surface of ITO- $\text{MnO}_2$  at a deposition time up to 60 s. The diameter of the metal oxide particles was  $200 \pm 50$  nm. For longer deposition times (i.e., 120 or 240 s) a  $\text{MnO}_2$  film is formed onto the surface instead of particles. It can be concluded that

particles caused better electrocatalytic behavior compared to the film, indicating a significant role in the morphology of MnO<sub>2</sub> deposits on their catalytic effect.

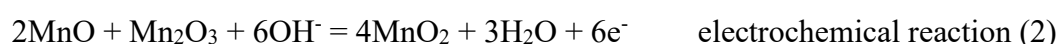
Please insert here Fig. 3a,3b, 3c, 3d

### 3.3. Effect of pH

The effect of pH on the oxidation peak potential of H<sub>2</sub>O<sub>2</sub> at ITO-MnO<sub>2</sub> and nanoSPCE-MnO<sub>2</sub> electrodes was investigated (Fig. 4).

Please insert here Fig. 4

A decrease in the anodic peak potential values from 1.0 to 0.6 V with increasing pH of the solution (in the presence of H<sub>2</sub>O<sub>2</sub>) was observed at both electrodes. The sharp potential shift corresponding to lower overpotentials for hydrogen peroxide oxidation was observed in the pH ranges 5-8 and 6-7, respectively at ITO-MnO<sub>2</sub> and nanoSPCE-MnO<sub>2</sub> electrodes. This indicates that hydroxyl ions play an important role in the electrocatalytic detection of H<sub>2</sub>O<sub>2</sub> at electrodes modified with MnO<sub>2</sub>. As the concentration of hydroxyl ions increases, the oxidation of manganese ions is going on easier. According to the literature [10], the scheme of the catalytic cycle of oxidation and reduction of hydrogen peroxide, can be assumed as follows:



Initially, a chemical reaction occurs with the oxidation of hydrogen peroxide and the reduction of manganese dioxide to the lower oxidation levels. Then electrochemical oxidation of Mn(II,III) to Mn(IV) occurs at the electrode surface. Thus an alkaline medium is required to make the process easier. The optimum pH for H<sub>2</sub>O<sub>2</sub> detection starts at 7 for nanoSCPE-MnO<sub>2</sub> while pH=8 is necessary to reach similar electrocatalytic effectiveness at ITO-MnO<sub>2</sub> electrode. It can be assumed that the optimal pH value slightly depends on the properties of the working electrode. Phosphate buffer of pH 8.0 was used for the determination of H<sub>2</sub>O<sub>2</sub> in the further studies.

### 3.4. Electrochemical characteristics of nanoSPCE, nanoSPCE-MnO<sub>2</sub>, ITO and ITO-MnO<sub>2</sub> electrodes

The cyclic voltammetric response of another redox probe ( $1 \cdot 10^{-3}$  M K<sub>3</sub>Fe(CN)<sub>6</sub>) was used to evaluate the electrochemical characteristics of the nano SPCE, nanoSPCE-MnO<sub>2</sub>, ITO and ITO-MnO<sub>2</sub> electrodes. It can help to compare the effect of MnO<sub>2</sub> particles on the electrochemical characteristics of the studied electrodes.

The effect of scan rate on the oxidation peak of  $1 \cdot 10^{-3}$  M K<sub>3</sub>Fe(CN)<sub>6</sub> was studied by cyclic voltammetry. The plot of peak current vs. square root of scan rate ( $v^{1/2}$ ) was linear over the whole studied range of scan the rate from 10 to 250 mV·s<sup>-1</sup> for both nanoSPCE-MnO<sub>2</sub> and ITO MnO<sub>2</sub> electrodes (see supplementary material, Figs. 4S&5S). This indicates a typical diffusion-controlled behavior of the studied systems. The electron transfer rate constant ( $k_s$ ) and the transfer coefficient ( $\alpha$ ) were calculated using the Laviron equation [45]. The results are presented in Table 1. The  $\alpha$  value is almost similar for all studied electrodes. The value of  $k_s$  increased twice on nanoSPCE-MnO<sub>2</sub> compared to ITO electrodes. This contributes to explain why MnO<sub>2</sub> on the SPCE significantly promoted the electrocatalytic detection of H<sub>2</sub>O<sub>2</sub>, as discussed above.

The effective surface area ( $A$ , cm<sup>2</sup>) of the modified electrodes was determined using the Randles-Sevcik equation [45]. Slight increase in the effective surface area of nanoSPCE-MnO<sub>2</sub> compare to bare SPCE is observed. This feature was even more pronounced for ITO-MnO<sub>2</sub> (i.e., almost 100 times increase compared to bare ITO), suggesting that MnO<sub>2</sub> particles substantially contribute to the large surface area of ITO-MnO<sub>2</sub> while the nanostructured carbon particles constituting the nanoSPCE electrode already possesses large surface area. Overall, the value of effective surface area of the SPCE-MnO<sub>2</sub> was 10 times larger than of ITO-MnO<sub>2</sub>.

Please insert here Table 1.

### 3.5. Effect of SiO<sub>2</sub> film

The ITO-MnO<sub>2</sub> and nanoSPCE-MnO<sub>2</sub> electrodes were covered with silica film using EAD technique. SEM image of the ITO-MnO<sub>2</sub>-SiO<sub>2</sub> is presented in Fig. 5. The film is highlighted in

light on the micrograph. The black part on the right is an edge of the film. The dark circles in the center can be ascribed to MnO<sub>2</sub> particles.

Please insert here Fig.5.

The stability of the analytical signal of H<sub>2</sub>O<sub>2</sub> at the electrodes covered with SiO<sub>2</sub> film was improved. The Both operational and long term stability of nanoSPCE-MnO<sub>2</sub>-SiO<sub>2</sub> (i.e., the analytical signal of H<sub>2</sub>O<sub>2</sub> at the electrodes covered with SiO<sub>2</sub> film) was improved compared to nanoSPCE-MnO<sub>2</sub>. The intensity decrease of the analytical signal for 30 successive detection scans in 0.5 mM H<sub>2</sub>O<sub>2</sub> was respectively 30% and 15% at nanoSPCE-MnO<sub>2</sub> and at nanoSPCE-MnO<sub>2</sub>-SiO<sub>2</sub> (see supplementary material, Fig. 6S). The analytical signal of H<sub>2</sub>O<sub>2</sub> diminished by four times at nanoSPCE-MnO<sub>2</sub> but only 20% at nanoSPCE-MnO<sub>2</sub>-SiO<sub>2</sub> after one month of testing.

The characteristics of the calibration graphs for the determination of H<sub>2</sub>O<sub>2</sub> by CV method using bare and MnO<sub>2</sub>-modified nanoSPCE and ITO electrodes, with and without silica film, are presented in the Table 2. The oxidation potentials of H<sub>2</sub>O<sub>2</sub> are similar for the electrodes modified with MnO<sub>2</sub> and MnO<sub>2</sub>-SiO<sub>2</sub>. The relative standard deviation ( $s_r$  values) of the analytical signal of 5·10<sup>-4</sup> M H<sub>2</sub>O<sub>2</sub> were found to be respectively 0.06 and 0.02 at nanoSPCE-MnO<sub>2</sub> and nanoSPCE-MnO<sub>2</sub>-SiO<sub>2</sub> electrodes (n=10, P=0.95).

Please insert here Table 2.

The lowest oxidation potential, widest linear range of calibration graph and lowest LOD for the determination of H<sub>2</sub>O<sub>2</sub> is observed for the nanoSPCE-MnO<sub>2</sub>-SiO<sub>2</sub>. This indicates not only that silica does not prevent the electrocatalytic properties of the MnO<sub>2</sub>-modified electrodes, but also contributes to improve somewhat their performance, which could be related to the fast mass transport properties featured by such mesoporous silica films [41,42].

### 3.6. Interference studies

The possible interference effect of ascorbic acid on the analytical signal of H<sub>2</sub>O<sub>2</sub> at the electrodes modified with MnO<sub>2</sub> was investigated. This compound is indeed present in biological

fluids, together with the target analyte, and can influence the results of its amperometric determination as it is expected to be oxidized in similar potential region. Equimolar amounts of ascorbic acid interfere on H<sub>2</sub>O<sub>2</sub> detection at the bare electrodes, especially at ITO (Fig. 6a). Such deleterious effect of ascorbic acid was substantially less at the electrodes modified with MnO<sub>2</sub> (Fig. 6c). It is interesting to note that the oxidation peak of ascorbic acid decreased with increasing scan rate from 25 to 100 mV·s<sup>-1</sup> at the ITO-MnO<sub>2</sub> while the oxidation current of H<sub>2</sub>O<sub>2</sub> was not noticeably changed (Fig. 6, compare a&b and c&d).

Please insert here Fig. 6 a, b, c, d

It can be a result of the differences in the kinetics of the oxidation of the studied compounds at metal oxide particles. The difference between oxidation current of H<sub>2</sub>O<sub>2</sub> and ascorbic acid was more important at a scan rate of 100 mV·s<sup>-1</sup>. The hydrogen peroxide can be determined in the presence of equimolar amounts of ascorbic acid at both nanoSPCE-MnO<sub>2</sub>-SiO<sub>2</sub> and ITO-MnO<sub>2</sub>-SiO<sub>2</sub> electrodes.

#### **4. Conclusions**

Nanostructured screen printed carbon (nanoSPCE) and ITO electrodes modified with MnO<sub>2</sub> by an electrodeposition method have demonstrated good electrocatalytic properties in the presence of H<sub>2</sub>O<sub>2</sub>. The uniformly distributed particles of MnO<sub>2</sub> obtained under optimal conditions provided high electrocatalytic currents for H<sub>2</sub>O<sub>2</sub> at nanoSPCE-MnO<sub>2</sub> and ITO-MnO<sub>2</sub> electrodes. Larger effective surface areas and faster charge transfer rates were observed at the nanoSPCE-MnO<sub>2</sub> electrode. This latter was characterized by lower LOD and wider linear range of the calibration curve for the determination of H<sub>2</sub>O<sub>2</sub> compared to ITO-MnO<sub>2</sub> electrode. The modification of MnO<sub>2</sub>-functionalized electrodes with a mesoporous silica film contributed to provide better stability of the analytical response of the studied electrodes. NanoSPCE-MnO<sub>2</sub>-SiO<sub>2</sub> is perspective element of amperometric sensor for the detection of hydrogen peroxide in the presence of equimolar amounts of ascorbic acid.

## Acknowledgement

One of the authors (O.T.) acknowledges a guest professorship fellow from the *Université de Lorraine* (France).

## References

- [1] Biosensors: Fundamentals and applications, Ed by A. Turner, I. Karube, G.W. Wilson, Oxford University Press., Oxford, New York, Tokio, (1987) 614.
- [2] G. Evtugyn, Biosensors: Essentials, Springer, Springer-Verlag Berlin Heidelberg (2014) 274 .
- [3] N. Thiyagarajan, J-L. Chang, K. Senthilkumar, J-M. Zen, Disposable electrochemical sensors: A mini review, *Electrochem. Commun.* 38 (2014) 86–90.
- [4] M. Pumera, S. Sanchez, I. Ichinose, J. Tang, Electrochemical nanobiosensors, *Sens. Actuators B* 123 (2007) 1195–1205.
- [5] T. Monteiro, M. Almeida, Electrochemical Enzyme Biosensors Revisited: Old Solutions for New Problems, *Crit. Rev. Anal. Chem.* (2018), in press (doi: 10.1080/10408347.2018.1461552).
- [6] J. Wang, Electrochemical glucose biosensors, *Chem. Rev.* 108 (2008) 814-825.
- [7] A. Liu, Towards development of chemosensors and biosensors with metal-oxide-based nanowires or nanotubes, *Biosens Bioelectron.* 24 (2008) 167-177.
- [8] R. Chinnasamy, G. M. Rao, R.T. Rajendra kumar, Synthesis and electrocatalytic properties of manganese dioxide for non-enzymatic hydrogen peroxide sensing, *Mater. Sci. Semicond. Process.* 31 (2015) 709-714.
- [9] E.P. Cicolatti, A. Valério, R.O. Henriques, D.E. Moritz, J.L. Ninow, D.M.G. Freire, E.A. Manoel, R. Fernandez-Lafuente, D. de Oliveira, Nanomaterials for biocatalyst immobilization – state of the art and future trends, *RSC Adv.* 6 (2016) 104675-104692.
- [10] N. W. Beyene, P. Kotzian, K. Schachl, H. Alemu, E. Turkušić, A. Copra, H. Moderegger, I. Švancara, K. Vytras, K. Kalcher, (Bio)sensors based on manganese dioxide-modified carbon substrates: retrospections, further improvements and applications, *Talanta* 64 (2004) 1151–1159.
- [11] E. A. Dontsova, I. A. Budashov, A. V. Eremenk, I. N. Kurochkin, Hydrogen Peroxide-Sensitive Amperometric Sensor Based on Manganese Dioxide Nanoparticles, *Nanotechnol. Russia* 3 (2008) 510–520.

- [12] E.A. Dontsova, Y.S. Zeifman, I.A. Budashov, A.V. Eremenko, S.L. Kalnov, I.N. Kurochkin, Screen-printed carbon electrode for choline based on MnO<sub>2</sub> nanoparticles and choline oxidase/polyelectrolyte layers. *Sens. Actuators B* 159 (2011) 261-270.
- [13] J.-J. Xu, X.-L. Luo, Y. Du, H.-Y. Chen, Application of MnO<sub>2</sub> nanoparticles as an eliminator of ascorbate interference to amperometric glucose biosensors, *Electrochem. Commun.* 6 (2004) 1169-1173.
- [14] S. H. Choi, S. D. Lee, J.H. Shin, J. Ha, H. Nam, G. S. Cha, Amperometric biosensors employing an insoluble oxidant as an interference-removing agent, *Anal. Chim. Acta* 461 (2002) 251-260.
- [15] I. Mazurenko, O. Tananaiko, O. Biloivan, M. Zhybak, I. Pelyak, V. Zaitsev, M. Etienne, A. Walcarius, Amperometric Biosensor for Choline Based on Gold Screen-Printed Electrode Modified with Electrochemically Deposited Silica Biocomposite, *Electroanalysis* 27 (2015) 1685–1692.
- [16] X. Liu, C. Chen, Y. Zhao, B. Jia, A Review on the Synthesis of Manganese Oxide Nanomaterials and Their Applications on Lithium-Ion Batteries, *J. Nanomater.* (2013) 736375.
- [17] Z. Taleat, A. Khoshroo, M. Mazloum-Ardakani, Screen-printed electrodes for biosensing: a review (2008–2013), *Microchim. Acta* 181 (2014) 865–891.
- [18] F. Arduini, L. Micheli, D. Moscone, G. Palleschi, S. Piermarini, F. Ricci, G. Volpe, Electrochemical biosensors based on nanomodified screen-printed electrodes: Recent applications in clinical analysis, *Trends Anal. Chem.* 79 (2016) 114–126.
- [19] F. Chekin, L. Gorton, I. Tapsobea, Direct and mediated electrochemistry of peroxidase and its electrocatalysis on a variety of screen-printed carbon electrodes: amperometric hydrogen peroxide and phenols biosensor, *Anal. Bioanal. Chem.* 407 (2015) 439–446.
- [20] K. Yamanaka, M. C. Vestergaard, E. Tamiya, Printable Electrochemical Biosensors: A Focus on Screen-Printed Electrodes and Their Application, *Sensors*, 16 (2016) 16.
- [21] S. Xu, X. Qin, X. Zhang, C. Zhang, A third-generation biosensor for hydrogen peroxide based on the immobilization of horseradish peroxidase on a disposable carbon nanotubes modified screen-printed electrode, *Microchim. Acta* 182 (2015)1241-1246.
- [22] Will be added
- [23] E. Turkusic, V. Milicevic, H. Tahmiscija, M. Vehabovic, S. Basic, V. Amidzic, Amperometric sensor for L-ascorbic acid determination based on MnO<sub>2</sub> bulk modified screen printed electrode, *Fresenius J. Anal. Chem.*, 368 (2000) 466–470.
- [24] N.W. Beyene, H. Moderegger, K. Kalcher, A Stable Glutamate Biosensor Based on MnO<sub>2</sub> Bulk-modified Screen-printed Carbon Electrode and Nafion Film-immobilized Glutamate Oxidase, *S. Afr. J. Chem.* 56 (2003) 54–59.

- [25] D. Telsnig, K. Kalcher, A. Leitner, A. Ortner, Design of an Amperometric Biosensor for the Determination of Biogenic Amines Using Screen Printed Carbon Working Electrodes, *Electroanalysis* 25 (2013) 47-50.
- [26] A. Abellán-Llobregat, I. Jeerapan, A. Bandothkar, L. Vidal, A. Canals, J. Wang, E. Morallón, A stretchable and screen-printed electrochemical sensor for glucose determination in human perspiration, *Biosens. Bioelectron.* 91 (2017) 885-891.
- [27] C. Guo H. Li, X. Zhang, H. Huo, C. Xu, 3D Porous CNT/MnO<sub>2</sub> Composite electrode for High-Performance Enzymeless Glucose Detection and Supercapacitor Application, *Sens. Actuators B* 206 (2015) 407-414.
- [28] S. Thiagarajan, T. H. Tsai, S-M. Chen, Electrochemical Fabrication of Nano Manganese Oxide Modified Electrode for the Detection of H<sub>2</sub>O<sub>2</sub>, *Int. J. Electrochem. Sci.* 6 (2011) 2235-2245.
- [29] G. Yu, Q. Zhao, W. Wu, X. Wei, Q. Lu, A facile and practical biosensor for choline based on manganese dioxide nanoparticles synthesized in-situ at the surface of electrode by one-step electrodeposition, *Talanta* 146 (2015) 707-713.
- [30] C. Roy Chaudhuri, A Review on Porous Silicon Based Electrochemical Biosensors: Beyond Surface Area Enhancement Factor, *Sens. Actuators B* 210 (2015) 310-323.
- [31] A. Walcarius, Template-directed porous electrodes in electroanalysis, *Anal. Bioanal. Chem.* 396 (2010) 261-272.
- [32] A. Walcarius, D. Mandler, J.A. Cox, M. Collinson, O. Lev, Exciting new directions in the intersection of functionalized sol-gel materials with electrochemistry, *J. Mater. Chem.* 15 (2005) 3663-3689.
- [33] G. Owens, R. Singh, F. Foroutan, M. Alqaysi, C.-M. Han, C. Mahapatra, H.-W Kim, J. C. Knowles Sol-gel based materials for biomedical applications, *Prog. Mater. Sci.* 77 (2016) 1-79.
- [34] M. M. Collinson, N. Moore, P. N. Deepa, M. Kanungo, Electrodeposition of porous silicate films from ludox colloidal silica, *Langmuir* 19 (2003) 7669-7672.
- [35] R. Shacham, D. Avnir, D. Mandler, Electrodeposition of Methylated Sol-Gel Films on Conducting Surfaces, *Adv. Mater.* 11 (1999) 384-388.
- [36] L. Liu, D. Mandler, Electrochemical Deposition of Sol-Gel Films, In L. Klein, M. Aparicio, A. Jitianu (eds) *Handbook of Sol-Gel Science and Technology*. Springer, Cham, (2016) pp. 1-38.
- [37] O. Nadzhafova, M. Etienne, A. Walcarius, Direct electrochemistry of hemoglobin and glucose oxidase in electrodeposited sol-gel silica thin films on glassy carbon, *Electrochem. Commun.* 9 (2007) 1189-1195.
- [38] A. Walcarius, E. Sibottier, M. Etienne, J. Ghanbaja, Electrochemically assisted self-assembly of mesoporous silica thin films, *Nature Mater.* 6 (2007) 602-608.



- [39] E. Sibottier, S. Sayen, F. Gaboriaud, A. Walcarius, Factors Affecting the Preparation and Properties of Electrodeposited Silica Thin Films Functionalized with Amine or Thiol Groups, *Langmuir* 22 (2006) 8366-8373.
- [40] D. Levy, M. Zayat, *The Sol-Gel Handbook - Synthesis, Characterization, and Applications, Synthesis and Processing*, Wiley-VCH (2015).
- [41] A. Goux, M. Etienne, E. Aubert, C. Lecomte, J. Ghanbaja, A. Walcarius, Oriented mesoporous silica films obtained by electro-assisted self-assembly (EASA), *Chem. Mater.* 21 (2009) 731-741.
- [42] M. Etienne, Y. Guillemin, D. Grosso, A. Walcarius, Electrochemical approaches for the fabrication and/or characterization of pure and hybrid templated mesoporous oxide thin films: a review, *Anal. Bioanal. Chem.* 405 (2013) 1497-1512.
- [43] N. Vila, J. Ghanbaja, E. Aubert, A. Walcarius, Electrochemically Assisted Generation of Highly Ordered Azide-Functionalized Mesoporous Silica for Oriented Hybrid Films, *Angew. Chem. Int. Ed.* 53 (2014) 2945-2950.
- [44] A. Maghear, M. Etienne, M. Tertiş, R. Sandulescu, A. Walcarius, Clay–mesoporous silica composite films generated by electro-assisted self-assembly, *Electrochim. Acta* 112 (2013) 333-341.
- [45] A.J. Bard, L.R. Faulkner, *Electrochemical Methods, Fundamentals and Applications*, 2nd ed., Wiley, New York, 2001.
- [46] J. Zbilji, V. Guzsvány, O. Vajdle, B. Prlina, J. Agbaba, B. Dalmacija, Z. Kónya, K. Kalche, Determination of H<sub>2</sub>O<sub>2</sub> by MnO<sub>2</sub> modified screen printed carbon electrode during Fenton and visible light-assisted photo-Fenton based removal of acetamiprid from water, *J. Electroanal. Chem.* 755 (2015) 77-86.

**Table 1.** Electrochemical characteristics of non modified and modified with MnO<sub>2</sub> ITO and nanoSPCE electrodes, n=3.

Electrode	$\alpha$	$k_s, s^{-1} \pm 0.05$	A, cm <sup>2</sup>
ITO	0.89	1.15	0.03
ITO-MnO <sub>2</sub>	0.89	1.16	2.70
nanoSPCE	0.86	2.50	15.30
nanoSPCE-MnO <sub>2</sub>	0.85	2.20	20.50

$k_s$  – charge transfer rate constant,  $\alpha$  - charge transfer coefficient, A - effective surface area.

**Table 2.** The characteristics of the calibration graphs for the determination of H<sub>2</sub>O<sub>2</sub> using different types of the electrodes

Electrode type	E <sub>ox</sub> (V)*	Linear range, mM	LOD (3s criteria), mM
ITO	0.65	2-11	1.8
ITO-MnO <sub>2</sub>	0.70	0.3-0.9	0.24
ITO-MnO <sub>2</sub> -SiO <sub>2</sub>	0.65	0.2-0.9	0.12
nanoSPCE	1.0	0.1-0.5	0.05
nanoSPCE-MnO <sub>2</sub>	0.6	0.05-1.0	0.025
nanoSPCE-MnO <sub>2</sub> -SiO <sub>2</sub>	0.6	0.02-1.0	0.01

\*E<sub>ox</sub> - the oxidation potential of hydrogen peroxide

### Figure caption

**Fig 1a.** CV curves recorded in the background electrolyte (1,3) and in the presence of  $1 \cdot 10^{-3}$  M  $H_2O_2$  (2,4) at non modified CSPE (1,2) and nanoSPCE (3,4); supporting electrolyte: 0.01 M PBS, pH = 8.5; scan rate 100 mV/s.

**Fig. 1b.** CV curves recorded in background electrolyte (1) and in the presence of  $1 \cdot 10^{-3}$  M  $H_2O_2$  (2) at nanoSPCE modified with  $MnO_2$  by electrodeposition procedure. Electrodeposition conditions: E= 0.8 V, time 60 s. Other conditions as in Fig. 1a.

**Fig. 2a.** CV curves recorded in the background electrolyte (1) and in the presence of  $1 \cdot 10^{-3}$  M  $H_2O_2$  (2) at bare ITO electrode. Other conditions as in Fig. 1a.

**Fig. 2b.** CV curves recorded in the background electrolyte (1) and in the presence of  $1 \cdot 10^{-3}$  M  $H_2O_2$  (2) at ITO modified with  $MnO_2$  by electrodeposition procedure. Other conditions as in Fig. 1b.

**Fig. 3a.** SEM image of bare ITO electrode surface.

**Fig. 3b.** SEM image of ITO- $MnO_2$  electrode surface; electrodeposition time 60 s, electrodeposition potential E=0.8 V.

**Fig. 3c.** SEM image of ITO- $MnO_2$  electrode surface; electrodeposition time 120 s, electrodeposition potential E=0.8 V.

**Fig. 3d.** SEM image of ITO- $MnO_2$  electrode surface; electrodeposition time 240 s, electrodeposition potential E=0.8 V.

**Fig. 4.** Effect of pH on the oxidation potential of  $1 \cdot 10^{-3}$  M  $H_2O_2$  at ITO- $MnO_2$  (1) and SPCE- $MnO_2$  (2); peak potentials obtained from CV curves recorded at a scan rate of 100 mV/s.

**Fig. 5.** SEM image of ITO- $MnO_2$ - $SiO_2$  electrode surface.

**Fig. 6 a,b.** CV curves recorded in the background electrolyte (1) and in the presence of  $1 \cdot 10^{-3}$  M  $\text{H}_2\text{O}_2$  (2) and  $1 \cdot 10^{-3}$  M ascorbic acid (3) at ITO; solution pH: 7.5; potential scan rates: 100 mV/s (a) and 25 mV/s (b).

**Fig. 6 c,d.** CV curves recorded in the background electrolyte (1) and in the presence of  $1 \cdot 10^{-3}$  M  $\text{H}_2\text{O}_2$  (2) and  $1 \cdot 10^{-3}$  M ascorbic acid (3) at ITO- $\text{MnO}_2$ - $\text{SiO}_2$ ; solution pH: 7.5; potential scan rates: 100 mV/s (c) and 25 mV/s (d).